

# ReactionMamba: Generating Short & Long Human Reaction Sequences

Hajra Anwar Beg<sup>1,2</sup>, Baptiste Chopin<sup>3</sup>, Hao Tang<sup>4</sup>, Mohamed Daoudi<sup>1,2</sup>

<sup>1</sup> Univ. Lille, CNRS, Centrale Lille, Institut Mines-Télécom, UMR 9189 CRISTAL, F-59000 Lille, France

<sup>2</sup> IMT Nord Europe, Institut Mines-Télécom, Univ. Lille, Centre for Digital Systems, F-59000 Lille, France

<sup>3</sup> da/sec – Biometrics and Security Research Group, Hochschule Darmstadt, Germany

<sup>4</sup> Peking University

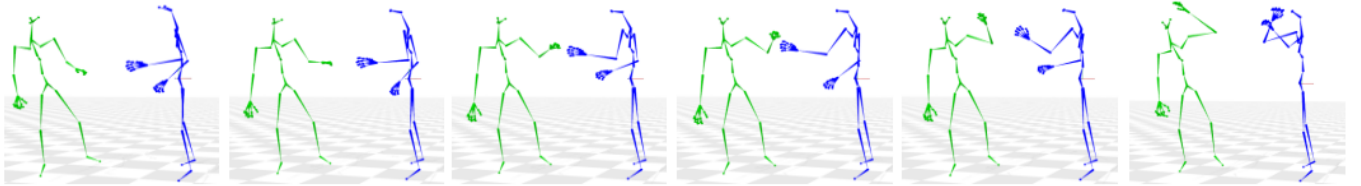


Fig. 1: Examples of reactive 3D motion generated with our proposed model for the NTU120-AS dataset Cheers and drink. Here we synthesize the 3D pose of the reactor (green) conditioned on the 3D motion of the actor (blue) and the initial pose of the reaction.

**Abstract**— We present ReactionMamba, a novel framework for generating long 3D human reaction motions. ReactionMamba integrates a motion VAE for efficient motion encoding with Mamba-based state-space models to decode temporally consistent reactions. This design enables ReactionMamba to generate both short sequences of simple motions and long sequences of complex motions, such as dance and martial arts. We evaluate ReactionMamba on three datasets—NTU120-AS, Lindy Hop, and InterX—and demonstrate competitive performance in terms of realism, diversity, and long-sequence generation compared to previous methods, including InterFormer, ReMoS, and Ready-to-React, while achieving substantial improvements in inference speed.

## I. INTRODUCTION

In recent years, there has been impressive progress in human motion generation under various user-specified conditions, such as music pieces [64] and text prompts [40]. However, most of these approaches focus on a single-person setting [7], [39] and, as a result, neglect one essential aspect of human motion: rich human-to-human interactions. One important aspect of human interaction is that the action of one person will usually elicit a reaction from another person. Synthesizing human-to-human interactions introduces advanced capabilities for character animation tools and software, with applications across commercial and entertainment media [24], interactive mixed and augmented reality [18], social robotics [59], and avatar interaction [8].

This led recent research to take interest in the task and propose various architectures to generate reaction motions [20], [9], [43]. However, human interaction reactions present a more challenging task due to the motion reactions, which are highly complex and have low periodicity. They require extremely accurate modeling of both spatial and temporal features, without which the generated motion looks

unrealistic. While current state-of-the-art methods can now generate reactive motion for simple and short actions they still struggle with longer sequences. Indeed short sequences often include simple motion such as boxing or kicking that can be more easily modeled due to a direct body contact leading to a clear reaction. Longer sequences however often include more complex interactions, such as dancing, where the relation between the action and the reaction is not always as direct and obvious. Modeling longer interaction sequences requires specific architectures, different from those focused on short sequences, to achieve high quality reaction generation. Precursor works on reaction generation have represented the task as a translation problem which directed them towards the Transformer [9]. However, this led to low diversity generation and limited performance in the long term. The self-attention mechanism computes interactions between every pair of tokens in the input sequence. This leads to quadratic time complexity in relation to the sequence length, which becomes a bottleneck for processing long sequences. As a result, it is essential to explore a new architectural paradigm that can handle long-range dependencies while maintaining linear computational complexity to support motion generation tasks. Recent advances have led to renewed interest in state-space models (SSMs) [23]. SSMs are a class of mathematical models used for modeling dynamic systems over time, often in fields like control theory, signal processing, and time series analysis. They have several advantages, particularly in their ability to model temporal dependencies for long sequences [23]. The efficiency in managing long sequences primarily due to its implementation of convolutional computations, which efficiently process sequential data. Convolutional operations

reduce the complexity associated with handling long-range dependencies by applying local filters to the sequence such as Mamba [22]. In this paper, we propose ReactionMamba (Figure 2) a new architecture for reaction motion generation that matches the state-of-the-art while increasing inference speed by a hundredfold. The Figure 1 shows some examples results obtained by our framework.

**Contributions.** Our contributions to the field of reaction motion generation can be summarized as:

- We introduce a simple yet effective framework, named ReactionMamba, which is a pioneering method integrates Mamba into human motion reaction generation.
- ReactionMamba is VAE [29] made up of three interconnected modules, an encoder, a conditioning module, and a decoder. The SSM based encoder encodes the reaction into a sequence of continuous latent variables in an efficient way, and a SSM based decoder is then designed to capture information hidden in the latent representations of the pose, combined with the action motion sequence and the initial frame of the reaction and to reconstruct the reaction.
- Unlike conventional deterministic methods, our method uses random latent sampling at inference, conditioned by the projected action sequence and the projected initial reaction pose, providing diverse and realistic reaction sequences.
- The ReactionMamba framework demonstrated exceptional performance on the action-reaction generation task for simple action-reaction categories [55] and [54], two-person interactions such as LindyHop dancing and Ninjutsu martial arts [20], and acrobats performing figures [52]. ReactionMamba achieved state-of-the-art generation quality, diversity while greatly improving processing speed.

## II. RELATED WORK

**Single-Person Human Motion Synthesis.** Single-human motion synthesis has seen remarkable progress in recent years. To cite some examples, conditional VAEs [39], [11] have been proposed to map textual descriptions to human motion. More recent approaches, such as EDGE [47] and Dancing to Music [30], introduce frameworks for the generation of music-conditioned motion. However, these methods often require additional conditions to effectively model emotional expressiveness. In addition, these approaches focus on the generation of single-human while ReactMamba learns the synchronization between two interacting individuals directly from one person’s motion, without the need for additional prompts or labels.

**Reactive Motion Generation.** Reactive motion generation focuses on generating human motion in response to external agents. Reactive motion generation is inherently more challenging than generating a single human motion sequence. In [58], a motion graph synthesis technique is proposed that generates gestures and body motions in a dyadic conversation. [26] proposed to represent dual-agent interactions as an optimal control problem, where the actions of the

initiating agent induce a cost topology over the space of reactive poses – a space in which the reactive agent plans an optimal pose trajectory. InterFormer [9] uses an interaction transformer with both spatial and temporal attention to generate reactive motions given some initial seed poses of both characters. It incorporates an interaction distance module that integrates softmax-scaled joint distances into the attention matrix. ReMoS [20] proposes a diffusion-based framework and incorporates spatio-temporal cross-attention and hand interaction aware cross-attention. These works primarily focused on generating high-quality short sequences spanning 2 to 5 seconds (around 50 frames), with InterFormer noting an accumulation of errors in longer sequence generation. Ready-to-React [66] introduces a framework that models two-character interactions through independent reactions using an auto-regressive diffusion approach. While Transformer-based approaches produce high-quality results, they face scalability challenges as the number of persons or frames increases, owing to the quadratic complexity of the attention mechanism. In contrast, our method leverages Mamba [21], [13], which alleviates this limitation

**State Space Models and Human Motion Synthesis.** Despite the well-known superiority of transformer-based architectures in vision tasks [48], [16], [63], [49], [51], [1], [65], [12], [14], [15], [56], [32], [33], [31], [61], [6], [37], [10], [5], [3], [4], one of their most critical limitations lies in the quadratic complexity of the self-attention mechanism, which results in prohibitive memory consumption and computational overhead when dealing with long sequences or high-resolution visual inputs. This constraint has motivated an increasing body of research aiming to develop alternative sequence modeling paradigms that retain the representational power of transformers while significantly reducing their computational burden.

In this context, state-space sequence models (SSMs), inspired by classical control theory, have recently emerged as a powerful and efficient family of architectures for sequential data modeling [21], [13]. Unlike transformers, which rely on pairwise attention, SSMs leverage parameterized state transitions to capture long-range dependencies in a linear-time manner. Mamba [21], for instance, introduces a selective SSM formulation that incorporates time-varying parameters into the state-space framework, together with a hardware-aware algorithm design, leading to substantial improvements in both training efficiency and inference scalability.

Thanks to these properties, SSMs have rapidly been adopted across a wide spectrum of visual tasks, ranging from video classification, comprehension, and segmentation [27], [38], [50], [57], to movie scene detection [28]. Their applications further extend to cross-modal and generative domains, including text-to-motion generation [62], image compression [60], dance video synthesis [44], and image segmentation [36], [41], [35], [53], demonstrating their versatility and growing impact in computer vision. Mamba has recently achieved state-of-the-art results in human motion synthesis by generating long, coherent motion sequences [62]. Building on this, [45] introduced Dyadic Mamba for text-

driven dyadic motion generation. Unlike prior approaches, ReactionMamba generates synchronized full-body and hand motions for the reactor using only the actor's 3D motion, requiring no extra labels or prompts.

### III. THE PROPOSED METHOD

We aim to generate high-quality *reaction motion sequences* that are temporally and semantically consistent with a given *action motion*. The model operates on 3D skeletal pose data, where each pose is a set of joint coordinates over time.

#### A. Formulation

Let us consider  $P_t$  the positions of  $k$  distinct joints at time  $t$ . Consequently, an action sequence  $P$  of  $T$  frames, can be described as a sequence  $P = \{P_1, P_2, \dots, P_T\}$ , where  $P_t \in \mathbb{R}^d$  and  $d=3 \times k$ , where  $P_t = [J_1(t), \dots, J_k(t)]$ , with  $k$  the number of joints in the skeleton, and  $J_i(t) = [x_i(t), y_i(t), z_i(t)]$  the 3D coordinates of joint  $i$ . The goal is to generate a reaction  $\mathbf{Y} = \{Y_1, Y_2, \dots, Y_T\}$ , a sequence of skeleton poses, from  $\mathbf{X} = \{X_1, X_2, \dots, X_T\}$ , a sequence representing the action motion.

The temporal spatial encoder encodes the reaction sequence  $\mathbf{Y}$  into a sequence of latent variables  $\mathbf{Z}$  through the variational posterior as formulated:

$$\mu, \log \sigma^2 = \mathcal{E}(\mathbf{Y}), \quad \mathbf{Z} = \mu + \epsilon \odot \sigma, \quad \epsilon \sim \mathcal{N}(0, I),$$

where  $\mathbf{Z} = \{\mathbf{Z}_1, \dots, \mathbf{Z}_T\}$ ,  $\mathbf{Z}_i \in \mathbb{R}^{d_z}$ .

The conditioning module maps the action sequence  $\mathbf{X}$  and the initial reaction pose  $Y_1$  to contextual embeddings  $X' \in \mathbb{R}^{T \times d_a}$  and  $Y'_1 \in \mathbb{R}^{T \times d_p}$  and then concatenates them with the latent  $\mathbf{Z}$ . The decoder receives the concatenated sequence  $[\mathbf{Z} \parallel X' \parallel Y'_1]$  and generates the full reaction motion  $\hat{\mathbf{Y}} \in \mathbb{R}^{T \times d}$ , through the following inverse process:

$$\hat{\mathbf{Y}} = \mathcal{D}(MLP([\mathbf{Z} \parallel Y' \parallel X'_1])).$$

#### B. Preliminaries

SSMs, particularly through the advancements of *Structured State Space Sequence Models (S4)* and *Mamba*, have demonstrated exceptional proficiency in modeling long sequences. A *Selective Structured State Space Sequence Model (S5)* is a neural sequence model derived from a discretized *linear time-invariant state space system*. Formally, let  $u(t)$  denote the input sequence at time  $t$ , and let  $h(t)$  denote the hidden state. The model maps  $u(t)$  to an output  $v(t)$  using  $\mathbf{A} \in \mathbb{R}^{N \times N}$  as the *state transition* (or evolution) matrix,  $\mathbf{B} \in \mathbb{R}^{N \times 1}$  and  $\mathbf{C} \in \mathbb{R}^{1 \times N}$  as the projection parameters, respectively. The discretized form of the system, incorporating a step size  $\Delta$ , is expressed as:

$$\begin{aligned} h_t &= \bar{\mathbf{A}}h_{t-1} + \bar{\mathbf{B}}u_t, \\ v_t &= \mathbf{C}h_t, \end{aligned} \tag{1}$$

where  $\bar{\mathbf{A}}$  and  $\bar{\mathbf{B}}$  are the discretized forms of  $\mathbf{A}$  and  $\mathbf{B}$ .

This formulation enables efficient computation via *global convolution*, leveraging a *structured convolutional kernel*  $\bar{\mathbf{K}}$

over the full input sequence of length  $M$ . The kernel is constructed as:

$$\begin{aligned} \bar{\mathbf{K}} &= \left( \bar{\mathbf{C}}\bar{\mathbf{B}}, \bar{\mathbf{C}}\bar{\mathbf{A}}\bar{\mathbf{B}}, \dots, \bar{\mathbf{C}}\bar{\mathbf{A}}^{M-1}\bar{\mathbf{B}} \right), \\ \mathbf{y} &= \mathbf{u} * \bar{\mathbf{K}}, \end{aligned} \tag{2}$$

where  $*$  denotes the *convolution operation* applied along the temporal dimension of the sequence.

We use Mamba modules as shown in Figure 2 inside both the encoder and decoder to handle temporal dependencies and capture long-range relationships in sequential data.

#### C. Model Architecture

The **encoder network** processes the input reaction motion sequence  $\mathbf{Y}$  by first passing it through a linear layer that projects each pose into a hidden dimension  $d_{model}$ . This projected sequence is then injected into a series of Mamba-based modules Figure 2, directly inspired by the original implementation [42]. Each block consists of a Mamba SSM and a gated multilayer perceptron (MLP) with  $d_{intermediate}$  hidden units. The first block receives as input the projected reaction sequence and produces hidden states and residuals that will be used as input of the next block. In each block residual connection fusion applied along with RMS normalization. Once the sequence has passed through all interconnected blocks, a final normalization and a linear projection are used to produce the encoder output of dimensions  $(T \times d_{model})$ .

The **decoder network** receives as input the latent vector  $\mathbf{Z}$  of dimension  $d_z$ , refined with a projection of the action motion sequence  $\mathbf{Y}$  and the initial pose  $Y_1$  to a space of size  $d_c$  for each via concatenation. Now this new input is projected to the hidden dimension  $d_{model}$ . The decoder architecture mirrors that of the encoder, using sequence of Mamba-based modules. Each block again applies a Mamba layer to capture the temporal structure of the input, followed by a gated MLP. Residual connections and RMS normalization are fused at both stages to maintain consistency with the encoder. After processing, a final normalization and linear projection produce the reconstructed reaction motion sequence  $\hat{\mathbf{Y}}$ .

#### D. Loss Functions

We use the reconstruction loss, the KL divergence loss, and reaction loss to optimize our model. The *reconstruction loss* (MSE) compares the generated reaction  $\hat{\mathbf{X}} \in \mathbb{R}^{T \times d}$  and the ground-truth reaction  $\mathbf{X} \in \mathbb{R}^{T \times d}$ . The loss of reconstruction,  $\mathcal{L}_{recon}$ , ensures that the generated reaction is perceptually and structurally similar to the generated reaction. The *KL divergence*  $\mathcal{L}_{KL}$  enforces latent variable distributions to follow a prior distribution. The KL divergence loss regularizes the latent space by encouraging it to conform to a prior distribution, ensuring smoothness and continuity in the learned latent representations. Finally, similar to [20], we define *reaction loss*  $\mathcal{L}_{react}$  which captures how closely each predicted reaction remains consistent with the actor's motion  $\mathbf{Y} \in \mathbb{R}^{T \times d}$ . The reaction loss encourages the physical consistency with the action motion and penalizes deviations

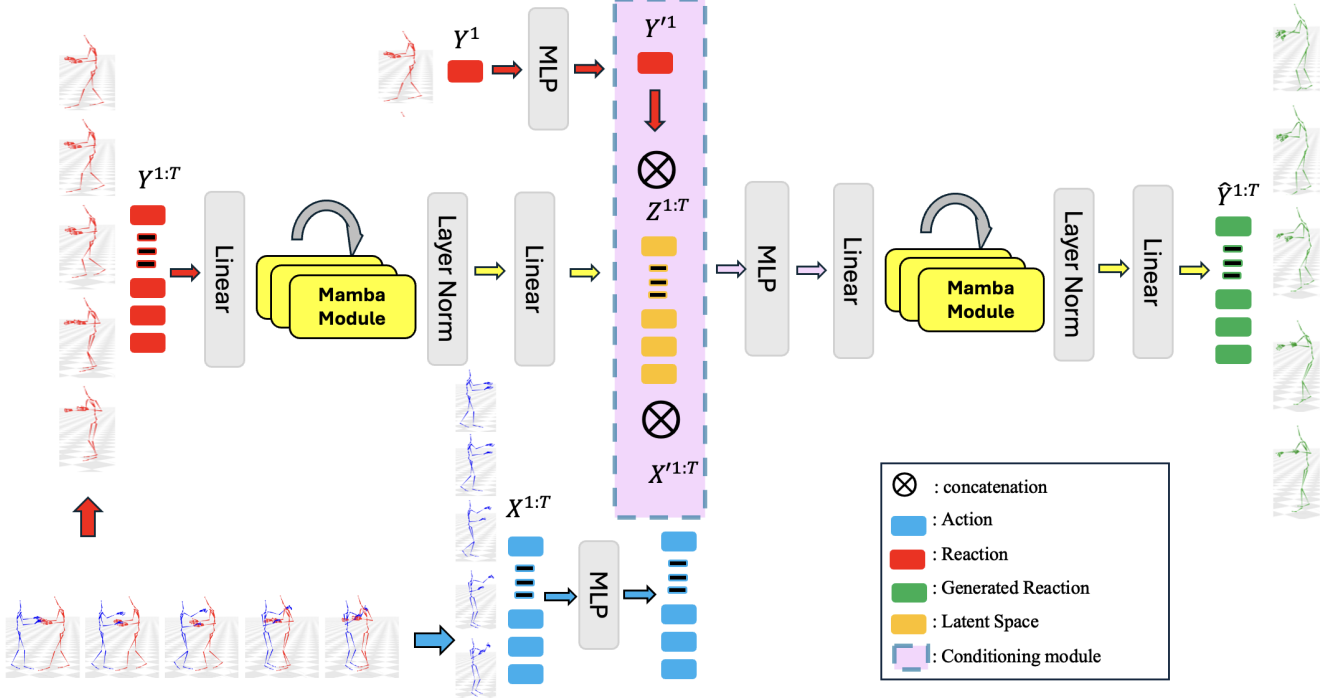


Fig. 2: **Architecture of ReactionMamba.** The Mamba encoder encodes the motion of the reaction  $\mathbf{Y}$  and maps it to a latent representation  $\mathbf{Z}$ . The decoder network takes as input the concatenation of the latent vector  $\mathbf{Z}$ , a projection of the action motion sequence  $\mathbf{X}$ , and the initial pose  $\mathbf{Y}_1$ , and produces the reconstructed reaction motion sequence  $\hat{\mathbf{Y}}$ .

from the expected motion difference in joint space. It is defined by:

$$\mathcal{L}_{\text{react}} = \frac{1}{T} \sum_{t=1}^T \exp(-\|\mathbf{Y}_t - \mathbf{X}_t\|_2) \times \left( \|\mathbf{Y}_t - \hat{\mathbf{X}}_t\|_2 - \|\mathbf{Y}_t - \mathbf{X}_t\|_2 \right)^2 \quad (3)$$

The total loss function is expressed as:

$$\mathcal{L} = w_{\text{recon}} \mathcal{L}_{\text{recon}} + w_{\text{KL}} \mathcal{L}_{\text{KL}} + w_{\text{react}} \mathcal{L}_{\text{react}}$$

#### IV. EXPERIMENTS

##### A. Datasets

We validated the proposed method in a broad set of experiments on 3 publicly available interaction datasets with 3D skeletons. **ReMoCap** [20] dataset consists of two types of two-person interactions: Lindy Hop dancing and Ninjutsu martial arts. **The Lindy Hop** subset comprises 8 dance motion sequences, each approximately 7.5 minutes long and recorded at 50 frames per second. We tested our method and the baselines on this subset of ReMoCap following the preprocessing and train/test split provided by the authors. **NTU120-AS** [55] is an annotated and extended version of the NTU RGB+D 120 dataset [34]. It contains 26 action categories, such

as “kick”, “push”, “hug”, and “finger guessing”. We used the same data processing as in [55]. **InterX** [54] is a large-scale dataset comprising 11,388 interaction sequences across 40 categories, such as “handshake”, “hug”, “pull”, and “point”. Each sequence is annotated with actor-reactor roles, making it well-suited for action–reaction modeling. We use the provided skeletons extracted from SMPL-X, apply downsampling, and construct our own train/test split.

##### B. Evaluation Metrics

To assess the fidelity and diversity of the generated reaction sequences  $\hat{\mathbf{Y}}$  compared to the ground truth  $\mathbf{Y}$ , we compute several quantitative metrics on the normalized data.

*a) Mean Per Joint Position Error (MPJPE):* MPJPE computes the average Euclidean distance between corresponding joints in the predicted and ground truth sequences. It is defined as:

$$\text{MPJPE} = \frac{1}{TJ} \sum_{t=1}^T \sum_{j=1}^J \left\| \hat{\mathbf{Y}}_{t,j} - \mathbf{Y}_{t,j} \right\|_2, \quad (4)$$

where  $T$  is the number of frames, and  $J$  is the number of joints. This metric evaluates the spatial accuracy of the predicted poses.

*b) Mean Per Joint Velocity Error (MPJVE):* MPJVE computes the average difference in joint velocities between

the predicted and ground truth sequences, capturing temporal consistency:

$$\text{MPJVE} = \frac{1}{(T-1)J} \sum_{t=1}^{T-1} \sum_{j=1}^J \left\| (\hat{Y}_{t+1,j} - \hat{Y}_{t,j}) - (Y_{t+1,j} - Y_{t,j}) \right\|_2. \quad (5)$$

c) *Fréchet Inception Distance (FID)*: FID allows to evaluate the quality of generated data by comparing the distribution of features extracted from real and generated sequences. After assuming these features follow multivariate Gaussian distributions with means and covariances  $(\mu, \Sigma)$  and  $(\hat{\mu}, \hat{\Sigma})$  respectively, FID is computed as:

$$\text{FID} = \|\mu - \hat{\mu}\|_2^2 + \text{Tr} \left( \Sigma + \hat{\Sigma} - 2(\Sigma \hat{\Sigma})^{1/2} \right). \quad (6)$$

A lower FID indicates that the generated data distribution closely matches the real data distribution, reflecting higher quality and diversity in the generated motions [17], [25].

d) *Diversity Metrics*: To specifically assess the diversity of the generated motions, we randomly sample pairs of motion sequences from feature space and compute the average Euclidean distance between them across frames and joints:

$$\text{Diversity}(S) = \frac{1}{|P|} \sum_{(i,j) \in P} \frac{1}{TJ} \sum_{t=1}^T \sum_{j=1}^J \left\| S_{t,j}^i - S_{t,j}^j \right\|_2, \quad (7)$$

where  $S^i$  and  $S^j$  are two sampled motion sequences from set  $S$  (either real or generated), and  $P$  is the set of randomly selected unique pairs. A diversity score close to the diversity score of the ground truth reflects greater variability within the motion set and a preservation of the original diversity.

### C. Baselines

We compare our method with three SOTA baselines, ReMoS [20], Interformer [9] both retrained on NVIDIA H100 SXM5 GPU (80 GB HBM3 VRAM) and Ready-to-React [2] trained on NVIDIA Quadro RTX 6000 GPU (24 GB VRAM). ReMoS [20] framework consists of two modules a body diffusion module and a hand diffusion module that need to be trained separately. We retrained ReMoS on each of the 3 datasets used in the experiments following instructions and recommendations from the authors github repository [19].

Interformer [9] is a Transformer-based model for reaction generation that we retrained on each of the 3 datasets used in the experiments following the protocol used by [20]. Ready-to-react [2], in contrast, employs an online reaction policy that conditions motion generation on the past trajectories of both interacting agents, enabling immediate and context-aware responses. In our experiments, we specifically adopt the reaction generation mode of Ready-to-React, which allows to generate the agents future movement based on its past history and the opponents motion. However, due to issues with preprocessing while following the protocol of the original implementation [66], we do not present results of Ready-to-React on the InterX dataset for the sake of fairness.

### D. Implementation

Reaction Mamba was trained using Adam optimizer. The base learning rate is set to  $10^{-4}$ , it decays following a Cosine Annealing LR scheduler. The input dimension is set to  $d = k \times 3$ ,  $d_{model} = 256$ ,  $d_z = 128$ ,  $d_{intermediate} = 512$ . We use 6 layers of the mamba block for both encoder and decoder. Before concatenation, the action and initial frame are projected to  $d_c = 64$  each of them. We set the loss weights,  $w_{\text{recon}} = w_{\text{recon}} = 1$  and  $w_{\text{KL}} = 0.5$ . Reaction Mamba was trained on NVIDIA Quadro RTX 6000 GPU (24 GB VRAM), for 300k iterations for Lindy Hop and 90K iterations for NTU120-AS and InterX.

## V. RESULTS

In this section, we present quantitative and qualitative results pertaining to reaction generation as well as a study of inference time. In each experiment, all models were trained on the dataset they are tested on. Each train set and test set was normalized following the definition in Section 3 of the supplementary material.

**Quantitative Results.** In Table I we present results on Lindy-Hop, and NTU120-AS, using each dataset default sequence length. We observe that ReactionMamba is competitive with the state-of-the-art on LindyHop across all metrics. Ready-to-React achieves the best MPJPE and MPJVE on these shorter sequences, showing its strength in short-horizon positional accuracy. However, its FID scores are considerably higher, revealing a lack of realism and consistency in longer rollouts. Meanwhile, we outperform all baselines on NTU120-AS, which can be explained by the lack of explicit contact information in this dataset. Indeed, this information is used by ReMoS to increase generation accuracy but is not needed by ReactionMamba. Another reason is ReactionMamba’s ability to better deal with sequences where the reactor does not move away from its original position (e.g. a sequence where two persons stand and shake hands). Our model is designed to inject the initial pose information at each frame in the conditioning module. Since the NTU120-AS dataset contains many such sequences, ReactionMamba is able to outperform InterFormer and Ready-to-React.

In Table II, we present results for long-term generation on the InterX dataset with 200-frame-long sequences. ReactionMamba clearly outperforms all baselines across metrics, generating accurate, smooth, and diverse long-horizon sequences. In contrast, ReMoS suffers from strong degradation, mainly because its spatio-temporal cross-attention mechanism requires very large memory. As a result, we had to reduce the batch size even when training on an NVIDIA H100 SXM5 GPU (80 GB HBM3 VRAM), which limited its performance. These results underline ReactionMamba’s robustness for stable and realistic long-term motion generation.

**Comparison of Inference Time.** We present in table III the inference time needed to generate 3840 sequences of 60 frames each. We show the total time to generate all sequences in minutes, the time to generate a single sequence in seconds and the number of frames generated per

TABLE I: Comparison of Results Across Different Datasets. **Bold** denotes the best results, while underline indicates the second-best results.

Lindy Hop (20 Frames $\sim 1s$ )				
Model	MPJPE	MPJVE	FID	$div_{gen}/div_{gt}$
ReMoS [20]	0.2194	<u>0.0033</u>	<u>2.3097</u>	<b>1.0021</b>
InterFormer [9]	0.1723	0.0046	2.7885	0.9936
Ready-to-React [66] (24 frames - 52 frames)	<b>0.1483</b>	<b>0.0031</b>	25.711	1.0032
ReactionMamba (Ours)	<u>0.1635</u>	<u>0.0037</u>	<b>1.9852</b>	<u>1.0025</u>
NTU120-AS (60 Frames $\sim 3s$ )				
Model	MPJPE	MPJVE	FID	$div_{gen}/div_{gt}$
ReMoS [20]	0.4577	0.0030	26.859	0.9654
InterFormer [9]	0.1865	<b>0.0020</b>	<u>5.9255</u>	1.0218
Ready-to-React [66]	0.5006	0.0037	12.292	<b>0.9872</b>
ReactionMamba (Ours)	<b>0.0922</b>	<u>0.0020</u>	<b>0.0321</b>	<u>0.9816</u>

TABLE II: Comparison of Results on long sequences generation. **Bold** denotes the best results, while underline indicates the second-best results.

InterX (200 Frames $\sim 10s$ )				
Model	MPJPE	MPJVE	FID	$div_{gen}/div_{gt}$
ReMoS [20]	0.3318	0.0033	51.272	0.7891
InterFormer [9]	0.2394	0.0025	6.1582	0.9329
ReactionMamba (Ours)	<b>0.0471</b>	<u>0.0007</u>	<b>0.0477</b>	<u>1.0026</u>

second (FPS). We see that ReactionMamba is much faster than the state-of-the-art, specifically 900 times faster than Ready-to-React, 1000 $\times$  faster than InterFormer, and more than 14,000 $\times$  faster than ReMoS. These results underline ReactionMamba’s efficiency, showing that it not only scales to large datasets but also enables real-time long-horizon generation.

TABLE III: Inference Speed on NVIDIA Quadro RTX 6000 for 3840 NTU-AS120 Sequences of 60 Frames each

Model	Total Time (min)	Time per Sequence (s)	FPS
ReMoS [20]	1691	26	2.3
Interformer [9]	122	1.9	32
Ready-to-React [66]	105	1.6	38
ReactionMamba (Ours)	<b>0.117</b>	<b>0.0018</b>	<b>33000</b>

**Qualitative Results.** We present in Figure 3 and Figure 4 visual results pertaining to long term retrogressive generation (1000 frames) on LindyHop and NTU120-AS push class respectively. Additional video results can be found in our supplementary material. In Figure 3 We observe that the qualitative results align well with the quantitative findings. The motion generated by ReactionMamba closely matches the ground truth and is comparable to Remos, while being hundreds of times faster. In contrast, Interformer’s motion loses coherence over time and fails to produce meaningful hand interactions. Similarly, Ready-to-React diverges after the first few hundred frames, with the reactor continuing its dance-like motion far away from the actor, and the generated hand motions becoming incoherent and poorly articulated. Meanwhile, in Figure 4 we see that ReactionMamba generate the best reaction to being pushed. Indeed, the other method

show less intense motion as well as penetration between the two bodies. Overall, these results clearly demonstrate the superior quality, stability, and efficiency of ReactionMamba compared to existing methods.

**Ablation.** We perform an ablation study to evaluate the influence of different components within our proposed ReactionMamba framework. We report ablation results in Table IV for LindyHop (20 frames). Five VAE variants are studied. **S1 (VAE + Mamba + Concat Action + Concat Init-Pose)** corresponds to our final model, where both the action stream and the initial pose are incorporated into the decoder via direct concatenation. **S2 (S1  $\rightarrow$  Replace Mamba with Attention)** keeps the same architecture as S1 but replaces all Mamba state space layers in the encoder and decoder with attention layers, which leads to significant degradation, especially in FID, confirming the effectiveness of Mamba for modeling long temporal dependencies. **S3 (S1  $\rightarrow$  Remove Init-Pose Concatenation)** removes the initial pose stream entirely in order to underline its necessity for generating consistent reaction motions. **S4 (S1  $\rightarrow$  Replace Init-Pose Concatenation with Gating)** introduces a dynamic gating mechanism, where the initial pose is injected into the latent sequence such that its influence gradually fades over time. While gating provides competitive performance, it consistently underperforms concatenation in reconstruction accuracy and stability, showing that directly concatenating the initial pose at every frame provides a stronger and more reliable conditioning signal. Finally, **S5 (S1  $\rightarrow$  Replace Action Concatenation with Cross-Attention)** replaces direct concatenation of the action stream with a cross-attention mechanism that enriches the latent sequence with action information. While cross-

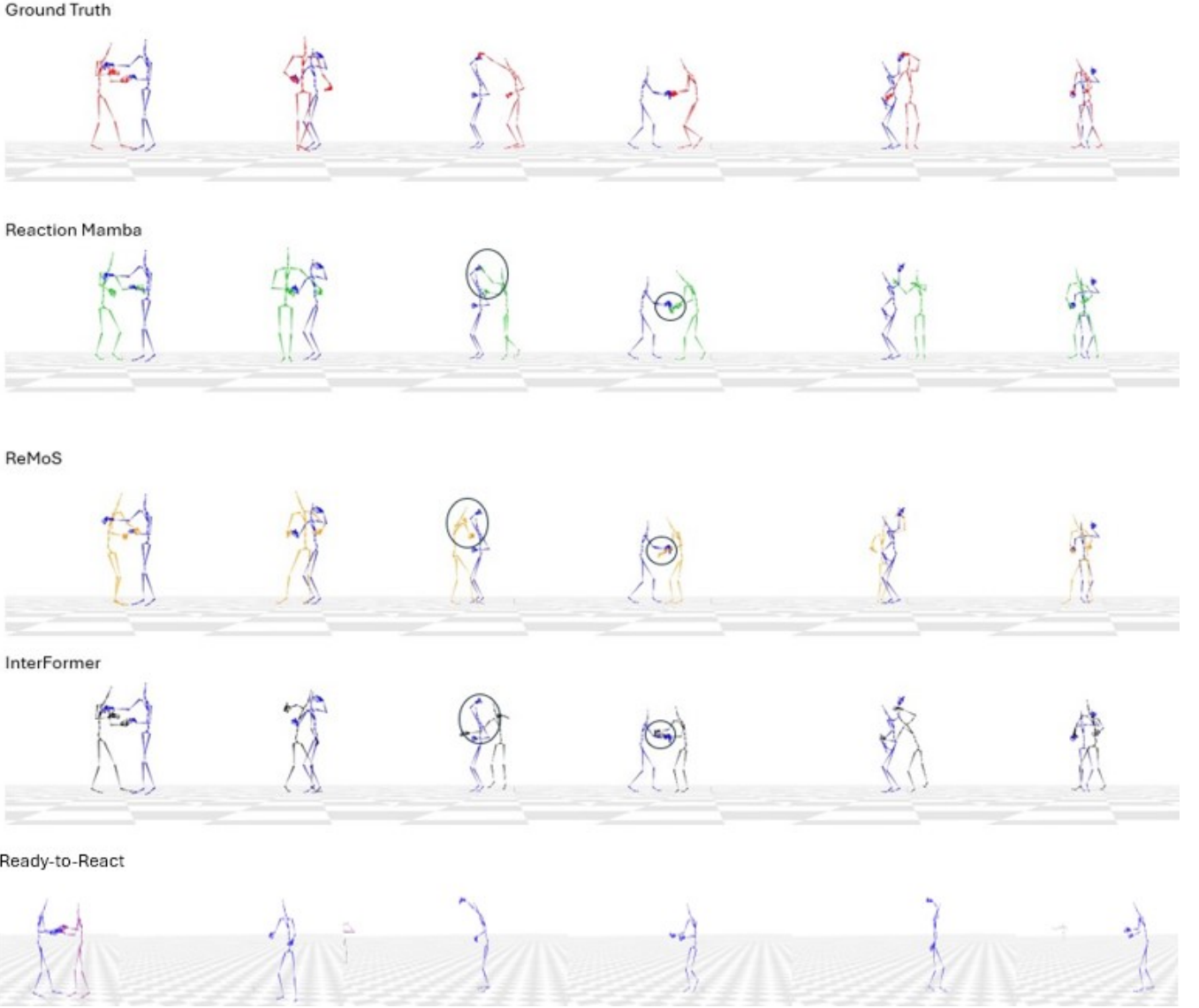


Fig. 3: Visualization of sequence generated on **Lindy Hop (1000 frames)**. In **blue** the action motion used as condition. In **red** the ground truth reaction and in other colors the reaction generated by the different models. See the supplementary material for their corresponding animations

attention yields slightly improved distributional realism in some cases, it comes at the cost of higher reconstruction errors, suggesting that action concatenation remains the more balanced and robust strategy overall. To conclude, for short sequences, concatenation clearly dominates (S1). For long sequences, gating or cross-attention can optimize a single metric (MPJPE or FID), but S1 offers the best overall balance of accuracy (MPJPE/MPJVE), distribution realism (FID), and stable diversity close to 1.0, while keeping the model simple, controllable, and robust to training instabilities. We therefore adopt S1 (VAE + Mamba + Concat(Action) + Concat(Init-Pose)) as our final architecture, and report S4/S5 as targeted alternatives when one metric (MPJPE or FID) is prioritized over the global trade-off.

Scenario	MPJPE $\downarrow$	MPJVE $\downarrow$	FID $\downarrow$	$div_{gen}/div_{gt}$
S1	<b>0.1634</b>	<b>0.00374</b>	<b>1.9852</b>	<b>1.0025</b>
S2	0.1833	0.00407	2.2392	1.0037
S3	0.2299	0.00543	2.3857	1.0157
S4	0.1773	0.00410	2.0318	0.9836
S5	0.2067	0.00427	2.0915	0.9925

TABLE IV: Ablation study on ReactionMamba. Results for LindyHop sequences of 20 frames each

## VI. LIMITATIONS AND FUTURE WORK

While ReactionMamba remains competitive with state-of-the-art methods and is considerably faster than previous approaches, it still exhibits certain limitations. Injecting initial

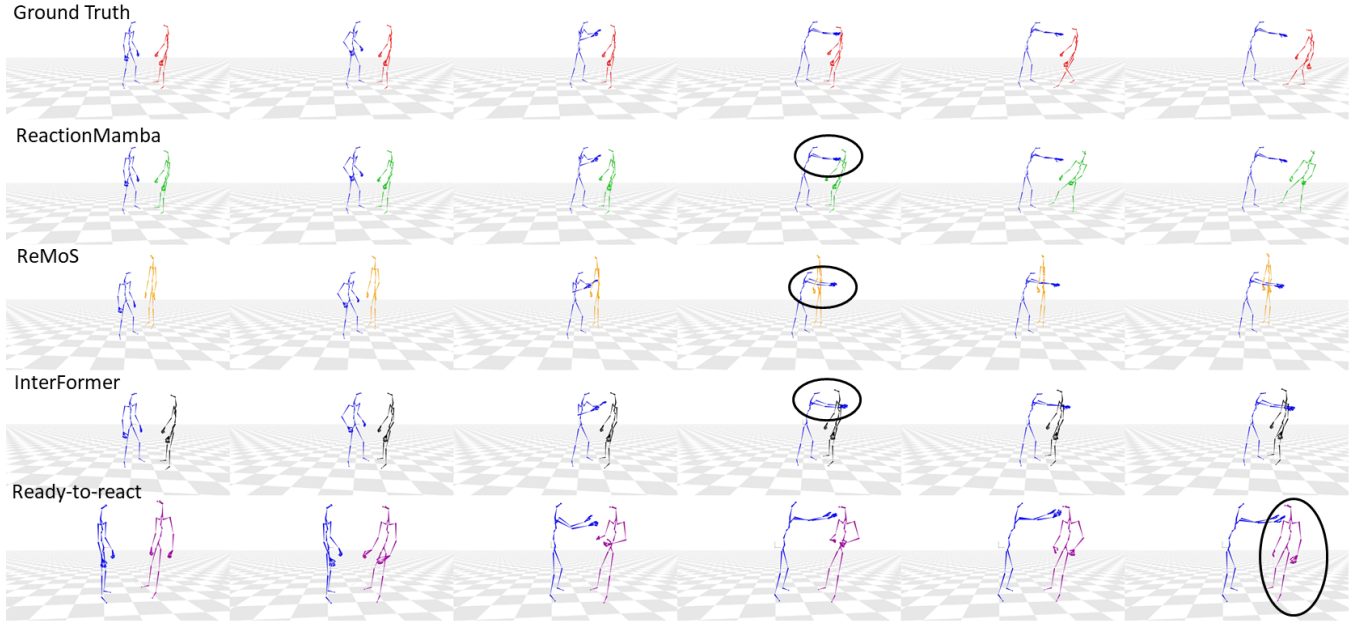


Fig. 4: Visualization of sequence generated on **NTU120-AS push class**. In **blue** the action motion used as condition. In **red** the ground truth reaction and in other colors the reaction generated by the different models. See the supplementary material for their corresponding animations

pose information at each frame into the conditioning module generally improves generation quality; however, the conditioning can sometimes be overly strong, leading to incorrect reactions (e.g., when the initial pose closely resembles that of a specific reaction) or even a lack of motion. In addition, like many existing models, ReactionMamba occasionally struggles to produce realistic leg movements, causing the character to “glide” rather than move naturally—particularly on the NTU120-AS dataset, where most actions and reactions are performed in place. In the future, to address these issues, we plan to adaptively weight the initial pose conditioning based on the type of action performed and its temporal progression. For instance, actions such as “Follow the other person” in NTU120-AS require the model to move significantly away from the initial pose. Thus, for such actions, the initial pose could be assigned greater importance at the beginning of the motion and gradually reduced over time. Furthermore, foot movement realism may be improved by incorporating a foot contact loss as proposed in [20], [46].

## VII. CONCLUSION

We present ReactionMamba, a new model for reaction generation. ReactionMamba adopts a VAE structure with an encoder and decoder based on the Mamba architecture. Extensive experiments on four datasets show that ReactionMamba is competitive with state-of-the-art methods both quantitatively and qualitatively for short-term and long-term reaction generation, while being up to 1000 times faster. This substantial increase in generation speed enables real-time use of ReactionMamba and opens a wider range of applications

than existing methods.

## ACKNOWLEDGEMENTS

This project is supported by a French government grant under the France 2030 program – ANR-22-EXEN-0004 (PEPR eNSEMBLE / PC3).

## REFERENCES

- [1] N. Carion, F. Massa, G. Synnaeve, N. Usunier, A. Kirillov, and S. Zagoruyko. End-to-end object detection with transformers. In *ECCV*, 2020.
- [2] Z. Cen, H. Pi, S. Peng, Q. Shuai, Y. Shen, H. Bao, X. Zhou, and R. Hu. Ready-to-react: Online reaction policy for two-character interaction generation. In *ICLR*, 2025.
- [3] H. Chen, H. Tang, N. Sebe, and G. Zhao. Aniformer: Data-driven 3d animation with transformer. In *BMVC*, 2021.
- [4] H. Chen, H. Tang, R. Timofte, L. Van Gool, and G. Zhao. Lart: Neural correspondence learning with latent regularization transformer for 3d motion transfer. In *NeurIPS*, 2023.
- [5] H. Chen, H. Tang, Z. Yu, N. Sebe, and G. Zhao. Geometry-contrastive transformer for generalized 3d pose transfer. In *AAAI*, 2022.
- [6] K. Chen, J. K. Chen, J. Chuang, M. Vázquez, and S. Savarese. Topological planning with transformers for vision-and-language navigation. In *CVPR*, 2021.
- [7] X. Chen, B. Jiang, W. Liu, Z. Huang, B. Fu, T. Chen, and G. Yu. Executing your commands via motion diffusion in latent space. In *Proceedings of the IEEE/CVF Conference on Computer Vision and Pattern Recognition*, pages 18000–18010, 2023.
- [8] B. Chopin, M. Daoudi, and A. Bartolo. Avatar reaction to multimodal human behavior. In G. L. Foresti, A. Fusello, and E. R. Hancock, editors, *Image Analysis and Processing - ICIAP 2023 Workshops - Udine, Italy, September 11-15, 2023, Proceedings, Part I*, volume 14365 of *Lecture Notes in Computer Science*, pages 494–505. Springer, 2023.
- [9] B. Chopin, H. Tang, N. Otberdout, M. Daoudi, and N. Sebe. Interaction transformer for human reaction generation. *IEEE Trans. Multim.*, 25:8842–8854, 2023.
- [10] B. Chopin, H. Tang, N. Otberdout, M. Daoudi, and N. Sebe. Interaction transformer for human reaction generation. *IEEE TMM*, 2023.

[11] R. Dabral, M. H. Mughal, V. Golyanik, and C. Theobalt. Mofusion: A framework for denoising-diffusion-based motion synthesis, 2022.

[12] L. Dai, H. Liu, H. Tang, Z. Wu, and P. Song. Ao2-detr: Arbitrary-oriented object detection transformer. *IEEE TCSVT*, 2022.

[13] T. Dao and A. Gu. Transformers are SSMs: Generalized models and efficient algorithms through structured state space duality. In *International Conference on Machine Learning (ICML)*, 2024.

[14] P. Dong, Z. Kong, X. Meng, P. Yu, Y. Gong, G. Yuan, H. Tang, and Y. Wang. Hotbev: Hardware-oriented transformer-based multi-view 3d detector for bev perception. In *NeurIPS*, 2023.

[15] P. Dong, Z. Kong, X. Meng, P. Zhang, H. Tang, Y. Wang, and C.-H. Chou. Speeddetr: Speed-aware transformers for end-to-end object detection. In *ICML*, 2023.

[16] A. Dosovitskiy, L. Beyer, A. Kolesnikov, D. Weissenborn, X. Zhai, T. Unterthiner, M. Dehghani, M. Minderer, G. Heigold, S. Gelly, et al. An image is worth 16x16 words: Transformers for image recognition at scale. In *ICLR*, 2021.

[17] D. Dowson and B. Landau. The fréchet distance between multivariate normal distributions. *Journal of Multivariate Analysis*, 12(3):450–455, 1982.

[18] A. Egges, G. Papagiannakis, and N. Magnenat-Thalmann. Presence and interaction in mixed reality environments. *Vis. Comput.*, 23(5):317–333, 2007.

[19] A. Ghosh. Remos: 3d-motion conditioned reaction synthesis for two-person interactions. <https://github.com/anindital27/ReMoS>, 2024.

[20] A. Ghosh, R. Dabral, V. Golyanik, C. Theobalt, and P. Slusallek. Remos: 3d motion-conditioned reaction synthesis for two-person interactions. In *European Conference on Computer Vision (ECCV)*, 2024.

[21] A. Gu and T. Dao. Mamba: Linear-time sequence modeling with selective state spaces. *arXiv preprint arXiv:2312.00752*, 2023.

[22] A. Gu and T. Dao. Mamba: Linear-time sequence modeling with selective state spaces, 2024.

[23] A. Gu, I. Johnson, K. Goel, K. Saab, T. Dao, A. Rudra, and C. Ré. Combining recurrent, convolutional, and continuous-time models with linear state space layers. In M. Ranzato, A. Beygelzimer, Y. Dauphin, P. Liang, and J. W. Vaughan, editors, *Advances in Neural Information Processing Systems*, volume 34, pages 572–585. Curran Associates, Inc., 2021.

[24] E. Hanser, P. Mc Kevitt, T. Lunney, and J. Condell. Scenemaker: Intelligent multimodal visualisation of natural language scripts. In L. Coyle and J. Freyne, editors, *Artificial Intelligence and Cognitive Science*, pages 144–153, Berlin, Heidelberg, 2010. Springer Berlin Heidelberg.

[25] M. Heusel, H. Ramsauer, T. Unterthiner, B. Nessler, and S. Hochreiter. Gans trained by a two time-scale update rule converge to a local nash equilibrium. In I. Guyon, U. V. Luxburg, S. Bengio, H. Wallach, R. Fergus, S. Vishwanathan, and R. Garnett, editors, *Advances in Neural Information Processing Systems*, volume 30. Curran Associates, Inc., 2017.

[26] D.-A. Huang and K. M. Kitani. Action-reaction: Forecasting the dynamics of human interaction. In D. Fleet, T. Pajdla, B. Schiele, and T. Tuytelaars, editors, *Computer Vision – ECCV 2014*, pages 489–504, Cham, 2014. Springer International Publishing.

[27] M. M. Islam and G. Bertasius. Long movie clip classification with state-space video models. In *ECCV*, 2022.

[28] M. M. Islam, M. Hasan, K. S. Athrey, T. Braskich, and G. Bertasius. Efficient movie scene detection using state-space transformers. In *CVPR*, 2023.

[29] D. P. Kingma and M. Welling. Auto-encoding variational bayes. In *2nd International Conference on Learning Representations (ICLR) 2014*, 2014.

[30] H.-Y. Lee, X. Yang, M.-Y. Liu, T.-C. Wang, Y.-D. Lu, M.-H. Yang, and J. Kautz. Dancing to music. In *NeurIPS*, 2019.

[31] W. Li, H. Liu, H. Tang, and P. Wang. Multi-hypothesis representation learning for transformer-based 3d human pose estimation. *Elsevier PR*, 141:109631, 2023.

[32] W. Li, H. Liu, H. Tang, P. Wang, and L. Van Gool. Mhformer: Multi-hypothesis transformer for 3d human pose estimation. In *CVPR*, 2022.

[33] K. Lin, L. Wang, and Z. Liu. End-to-end human pose and mesh reconstruction with transformers. In *CVPR*, 2021.

[34] J. Liu, A. Shahroudy, M. Perez, G. Wang, L.-Y. Duan, and A. C. Kot. NTU RGB+D 120: A Large-Scale Benchmark for 3D Human Activity Understanding. *IEEE Transactions on Pattern Analysis and Machine Intelligence*, 42(10):2684–2701, 2020.

[35] J. Liu, H. Yang, H.-Y. Zhou, Y. Xi, L. Yu, Y. Yu, Y. Liang, G. Shi, S. Zhang, H. Zheng, et al. Swin-umamba: Mamba-based unet with imagenet-based pretraining. *arXiv preprint arXiv:2402.03302*, 2024.

[36] J. Ma, F. Li, and B. Wang. U-mamba: Enhancing long-range dependency for biomedical image segmentation. *arXiv preprint arXiv:2401.04722*, 2024.

[37] D. Neimark, O. Bar, M. Zohar, and D. Asselmann. Video transformer network. In *ICCV*, 2021.

[38] E. Nguyen, K. Goel, A. Gu, G. Downs, P. Shah, T. Dao, S. Baccus, and C. Ré. S4nd: Modeling images and videos as multidimensional signals with state spaces. In *NeurIPS*, 2022.

[39] M. Petrovich, M. J. Black, and G. Varol. TEMOS: Generating diverse human motions from textual descriptions. In *European Conference on Computer Vision (ECCV)*, 2022.

[40] M. Petrovich, M. J. Black, and G. Varol. TMR: Text-to-motion retrieval using contrastive 3D human motion synthesis. In *International Conference on Computer Vision (ICCV)*, 2023.

[41] J. Ruan and S. Xiang. Vm-unet: Vision mamba unet for medical image segmentation. *arXiv preprint arXiv:2402.02491*, 2024.

[42] S. Spaces. Mamba. <https://github.com/state-spaces/mamba>, 2023.

[43] K. Sui, A. Ghosh, I. Hwang, J. Wang, and C. Guo. A survey on human interaction motion generation, 2025.

[44] H. Tang, L. Shao, Z. Zhang, L. Van Gool, and N. Sebe. Spatial-temporal graph mamba for music-guided dance video synthesis. *IEEE TPAMI*, 2025.

[45] J. Tanke, T. Shibuya, K. Uchida, K. Saito, and Y. Mitsuishi. Dyadic mamba: Long-term dyadic human motion synthesis. In *IEEE/CVF Conference on Computer Vision and Pattern Recognition Workshops, CVPR Workshops 2025, Nashville, TN, USA, June 11–15, 2025*, pages 2868–2877. Computer Vision Foundation / IEEE, 2025.

[46] G. Tevet, S. Raab, B. Gordon, Y. Shafir, D. Cohen-or, and A. H. Bermano. Human motion diffusion model. In *The Eleventh International Conference on Learning Representations*, 2023.

[47] J. Tseng, R. Castellon, and K. Liu. Edge: Editable dance generation from music. In *CVPR*, 2023.

[48] A. Vaswani, N. Shazeer, N. Parmar, J. Uszkoreit, L. Jones, A. N. Gomez, L. Kaiser, and I. Polosukhin. Attention is all you need. In *NeurIPS*, 2017.

[49] H. Wang, Y. Zhu, H. Adam, A. Yuille, and L.-C. Chen. Max-deeplab: End-to-end panoptic segmentation with mask transformers. In *CVPR*, 2021.

[50] J. Wang, W. Zhu, P. Wang, X. Yu, L. Liu, M. Omar, and R. Hamid. Selective structured state-spaces for long-form video understanding. In *CVPR*, 2023.

[51] W. Wang, C. Chen, M. Ding, H. Yu, S. Zha, and J. Li. Transbts: Multimodal brain tumor segmentation using transformer. In *MICCAI*, 2021.

[52] G. Wen, B. Xiaoyu, A.-P. Xavier, and M.-N. Francesc. Multi-person extreme motion prediction. In *Proceedings of the IEEE International Conference on Computer Vision and Pattern Recognition (CVPR)*, 2022.

[53] Z. Xing, T. Ye, Y. Yang, G. Liu, and L. Zhu. Segmamba: Long-range sequential modeling mamba for 3d medical image segmentation. *arXiv preprint arXiv:2401.13560*, 2024.

[54] L. Xu, X. Lv, Y. Yan, X. Jin, S. Wu, C. Xu, Y. Liu, Y. Zhou, F. Rao, X. Sheng, et al. Inter-x: Towards versatile human-human interaction analysis. In *CVPR*, pages 22260–22271, 2024.

[55] L. Xu, Y. Zhou, Y. Yan, X. Jin, W. Zhu, F. Rao, X. Yang, and W. Zeng. Regennet: Towards human action-reaction synthesis. In *CVPR*, pages 1759–1769, 2024.

[56] G. Yang, H. Tang, M. Ding, N. Sebe, and E. Ricci. Transformer-based attention networks for continuous pixel-wise prediction. In *ICCV*, 2021.

[57] Y. Yang, Z. Xing, and L. Zhu. Vivim: a video vision mamba for medical video object segmentation. *arXiv preprint arXiv:2401.14168*, 2024.

[58] Y. Yang, J. Yang, and J. Hodgins. Statistics-based motion synthesis for social conversations. In *Proceedings of the 2020 ACM SIGGRAPH/Eurographics symposium on Computer animation*, 2020.

[59] Y. Yoon, W. Ko, M. Jang, J. Lee, J. Kim, and G. Lee. Robots learn social skills: End-to-end learning of co-speech gesture generation for humanoid robots. In *International Conference on Robotics and Automation, ICRA 2019, Montreal, QC, Canada, May 20–24, 2019*, pages 4303–4309. IEEE, 2019.

[60] F. Zeng, H. Tang, Y. Shao, S. Chen, L. Shao, and Y. Wang. Mambaic: State space models for high-performance learned image compression. In *CVPR*, 2025.

[61] Y. Zeng, J. Fu, and H. Chao. Learning joint spatial-temporal transformations for video inpainting. In *ECCV*, 2020.

[62] Z. Zhang, A. Liu, I. Reid, R. Hartley, B. Zhuang, and H. Tang. Motion

mamba: Efficient and long sequence motion generation. In *ECCV*, 2024.

- [63] S. Zheng, J. Lu, H. Zhao, X. Zhu, Z. Luo, Y. Wang, Y. Fu, J. Feng, T. Xiang, P. H. Torr, et al. Rethinking semantic segmentation from a sequence-to-sequence perspective with transformers. In *CVPR*, 2021.
- [64] Z. Zhou and B. Wang. Ude: A unified driving engine for human motion generation. In *2023 IEEE/CVF Conference on Computer Vision and Pattern Recognition (CVPR)*, pages 5632–5641, 2023.
- [65] X. Zhu, W. Su, L. Lu, B. Li, X. Wang, and J. Dai. Deformable detr: Deformable transformers for end-to-end object detection. In *ICLR*, 2021.
- [66] ZJU3DV. `ready_to_react`. [https://github.com/zju3dv/ready\\_to\\_react.git](https://github.com/zju3dv/ready_to_react.git), 2025.